SELF-SIMILAR RADIATION-HYDRODYNAMICS SOLUTIONS IN THE EQUILIBRIUM DIFFUSION LIMIT

An Undergraduate Research Scholars Thesis

by

TAYLOR KINSEY LANE

Submitted to Honors and Undergraduate Research
Texas A&M University
in partial fulfillment of the requirements for the designation as

UNDERGRADUATE RESEARCH SCHOLAR

Approved by
Research Advisor: Dr. Ryan G. McClarren

May 2013

Major: Nuclear Engineering

TABLE OF CONTENTS

ABSTRACT

Self-Similar Radiation-Hydrodynamics
Solutions in the Equilibrium Diffusion Limit. (May 2013)

Taylor Kinsey Lane
Department of Nuclear Engineering
Texas A&M University

Research Advisor: Dr. Ryan G. McClarren
Department of Nuclear Engineering

This work presents semi-analytical solutions to a radiation-hydrodynamics problems of a radiation source driving an initially cold medium. Our solutions are in the equilibrium diffusion limit, include material motion and allow for radiation-dominated situations where the radiation energy is comparable to (or greater than) the material internal energy density. As such, this work is a generalization of the classical Marshak wave problem that assumes no material motion and that the radiation energy is negligible. Including radiation energy density in the model serves to slow down the wave propagation. The solutions provide insight into the impact of radiation energy and material motion, as well as present a novel verification test for radiation transport packages. As a verification test, the solution exercises the radiation-matter coupling terms and their v/c treatment without needing a hydrodynamics solve. An example comparison between the self-similar solution and a numerical code is given. Tables of the self-similar solutions are also provided.

DEDICATION

I would like to thank my dad for constantly requiring excellence from me. Without his relentless motivation I would have never met the high goals I set for myself nor would I have embarked on this journey to write a thesis.

ACKNOWLEDGMENTS

I would like to thank Dr. Ryan McClarren for giving me the chance to work for him so early in my academic career. The knowledge you have shared with me in the past two years is invaluable and I'm personally grateful for you allowing me borrow your books for extended periods of time. I would also like to thank the Undergraduate Summer Research Grant (USRG) Program, Research Opportunities in Engineering (ROE) Scholars Program, and the Undergraduate Research Scholars Program (URSP) for funding me, my research, and my travels.

NOMENCLATURE

ODE	Ordinary Differential Equation
RHD	Radiation Hydrodynamics
HEDP	High-Energy Density Physics
PDE	Partial Differential Equation
LTE	Local Thermodynamics Equilibrium

CHAPTER I

INTRODUCTION

In today's scientific community, computer simulation has become an essential part of the scientific process. Simulation is involved in all aspects of research: theoretical, analytical, and experimental. Codes are now expected to produce accurate results for highly complex problems. The most interesting and relevant problems cannot have an analytical solution due to their inherent complexity in geometry, boundary conditions, or materials. To have confidence in a code used to solve these complicated problems, the codes need to be able to produce answers that can be verified for easier, known problems [1]. The downfall of this procedure is that errors can occur only in the more complex code, while performing flawlessly in the easier benchmark. This engenders a false sense of confidence, and subsequently accuracy, in simulation codes, due to no other solutions being available, no one can refute the accuracy of the simulation codes. To keep computer simulation involved in the scientific process, their reliability and accuracy must continue to improve. Because of this predicament, benchmark solutions are continually expected to model more complex problems as the state of the science advances. As the benchmark problems evolve and become more complex, the best one can hope to achieve are semi-analytic solutions. The solutions provided in this work are semi-analytic in nature. This term means the results are purely analytic, but the integration and ordinary differential equation (ODE) solver both use numerical methods. Therefore, the results are inherently analytic, but to obtain values, numerical methods are used.

Equations of Radiation Hydrodynamics

Radiation Hydrodynamics (RHD), at its most basic, can be described as a set of techniques used to understand a moving, radiating fluid. The field of RHD is often associated with High-

Energy Density Physics (HEDP). HEDP is a regime of computational physics loosely defined as the study of matter with energy densities that are orders of magnitudes greater than the energy density found at room temperature. Many of the phenomena studied in these fields involve any combination of plasmas, ions, radiation, and shock waves. These phenomena can be found in supernovae explosions, or in inertial confinement fusion applications.

Hydrodynamics Model

To begin to understand the complex flows involved with RHD, it is important to first consider hydrodynamics without any radiation. The Euler equations govern this flow and are given by,

$$\frac{\partial \rho}{\partial t} + \nabla \cdot (\rho \vec{v}) = 0 \,, \tag{I.1a}$$

$$\frac{\partial}{\partial t}(\rho v) + \nabla \cdot (\rho \vec{v} \otimes \vec{v}) + \nabla p = -\mathbb{P} S_{\mathrm{F}} \,, \tag{I.1b}$$

$$\frac{\partial}{\partial t}(\rho E) + \nabla \cdot [(\rho E + p)\, \vec{v}] = -\mathbb{C}\mathbb{P} S_{\mathrm{E}} \,, \tag{I.1c}$$

where ρ is the material density, $\vec{v}$ is the relative velocity, and p is the pressure. E, the total specific energy is given by

$$E = e + \frac{1}{2} v^2 \tag{I.2}$$

where $v = |\vec{v}|$ and e is the internal specific energy. $\mathbb{C}$ and $\mathbb{P}$ are non dimensional constants and S_{E} and S_{F} are source terms that are defined in detail in the next section, Radiative Transfer. An equation of state is also needed to close the system and will be defined later in this work. In particular, Equations (I.1a), (I.1b), (I.1c) represent the conservation of mass, momentum, and energy of the fluid, respectively. The Euler equations govern inviscid flows only. These are flows in which viscous effects are negligible and therefore not taken into consideration. Conversely, there are flows in High-Energy Density Physics in which this approximation fails. They typically occur in situations where the Euler equations present discontinuous solutions. Discontinuities can occur in shock waves and certain astrophysical situations, and should be

modeled with viscous effects included. However, this approximation is perfectly valid in the flows described in depth within this work.

Radiative Transfer

Radiation is a mechanism of energy and momentum transfer that is governed by highly non-linear partial differential equations (PDEs). The non-dimensional transfer equation for photons is given by

$$\left(\frac{1}{\mathbb{C}}\frac{\partial}{\partial t} + \mathbf{n}\cdot\nabla\right) I(\nu,\mathbf{n}) = S(\nu,\mathbf{n})\,, \tag{I.3}$$

where $I\left(\nu,\mathbf{n}\right)$ is the spectrally-dependent photon intensity, $S\left(\nu,\mathbf{n}\right)$ is the spectrally-dependent source term, and $\mathbb{C}$ is the ratio of the speed of light to the speed of sound in the medium. Mathematically, $\mathbb{C} = c/a_\infty$. $\mathbb{C}$ is a measure of how quickly the fluid responds to radiation effects in comparison to material effects and can be thought of as a relativistic parameter. $S(\nu,\mathbf{n})$, the source term, results from material interaction. This term has cross-sections embedded within it and can become rather burdensome depending on the frame used. This particular equation utilizes the Eulerian frame exclusively, with each variable's dependence on space and time suppressed [2]. Deriving both the Eulerian or comoving frame equations have been covered extensively in literature [3, 4], and therefore will not be explained in this study. For simplicity, spectrally averaged cross-sections are utilized (gray approximation), local thermodynamic equilibrium (LTE) is assumed, and scattering is neglected. These approximations maintain solution accuracy to $O(v/\mathbb{C})$ in the nonrelativistic HEDP regime [2].

P_1 Equations

The first three angular moments of $I(\nu,\mathbf{n})$ are defined as:

$$E_{\mathrm{r}} = \frac{1}{\mathbb{C}}\int_0^\infty d\nu \oint_{\mathbf{n}} d\mathbf{n}\, I(\nu,\mathbf{n}), \tag{I.4a}$$

$$F_{\mathrm{r}} = \int_0^\infty d\nu \oint_{\mathbf{n}} d\mathbf{n}\, \mathbf{n} I(\nu, \mathbf{n}), \tag{I.4b}$$

$$P_{\mathrm{r}} = \frac{1}{\mathbb{C}} \int_0^\infty d\nu \oint_{\mathbf{n}} d\mathbf{n}\, \mathbf{n} \otimes \mathbf{n} I(\nu, \mathbf{n}). \tag{I.4c}$$

Where E_{r} is the energy density, F_{r} is the radiation flux, P_{r} is the radiation pressure and $\mathbf{n}$ is the direction [5]. Assuming a one-dimensional Cartestian geometry gives $\mathbf{n} = \mu$ where $\mu = \cos(\theta)$. θ is the angle between the photon flight and the positive x-axis. The source terms are given by:

$$S_{\mathrm{E}} = \int_0^\infty d\nu \oint_{\mathbf{n}} d\mathbf{n}\, S(\nu, \mathbf{n}), \tag{I.5a}$$

$$S_{\mathrm{F}} = \frac{1}{\mathbb{C}} \int_0^\infty d\nu \oint_{\mathbf{n}} d\mathbf{n}\, \mathbf{n} S(\nu, \mathbf{n}). \tag{I.5b}$$

Taking the $\{1, \mathbf{n}\}$-angular moments of Equation (I.3), as shown above, and substituting the source term relationships gives:

$$\frac{\partial E_{\mathrm{r}}}{\partial t} + \mathbb{C}\nabla \cdot F_{\mathrm{r}} = \mathbb{C} S_{\mathrm{E}}, \tag{I.6a}$$

$$\frac{\partial F_{\mathrm{r}}}{\partial t} + \frac{1}{3}\mathbb{C}\nabla E_{\mathrm{r}} = \mathbb{C} S_{\mathrm{F}}, \tag{I.6b}$$

$$\frac{\partial \rho e}{\partial t} = -\mathbb{P}\mathbb{C} S_{\mathrm{E}}. \tag{I.6c}$$

where

$$S_{\mathrm{E}} = \sigma(T^4 - E_{\mathrm{r}}) + \sigma \frac{v}{\mathbb{C}} \cdot F_{\mathrm{r0}}, \tag{I.7a}$$

$$S_{\mathrm{F}} = -\sigma F_{\mathrm{r0}} + \sigma \frac{v}{\mathbb{C}}(T^4 - E_{\mathrm{r}}), \tag{I.7b}$$

$$F_{\mathrm{r0}} = F_{\mathrm{r}} - (v E_{\mathrm{r}} + \frac{v}{3} E_{\mathrm{r}})/\mathbb{C}. \tag{I.7c}$$

These are the P_1 equations generalized for one-dimensional radiation transport. Their name comes from the approximation used to close the system, $P_{\mathrm{r}} = \frac{1}{3} E_{\mathrm{r}}$. This approximation is obtained when a first-order (hence the name) Legendre expansion is assumed for $I(\mathbf{n})$. For

a more detailed explanation of their derivation, please refer to [5]. It is beneficial to work with non dimensional variables so the following nondimensionalization scheme is proposed:

$$\hat{t} = \frac{t\ell}{a_\infty} \qquad \hat{u} = a_\infty u \qquad \hat{x} = x\ell \qquad e = \frac{\hat{e}}{c_v T_\infty} = \frac{c_v \hat{T}}{c_v T_\infty} \qquad T = \frac{\hat{T}}{T_\infty}.$$

where hatted variables $(\hat{\cdot})$ denote a dimensional quantity and the subscript infinity describes a flow scale or a characteristic/reference quantity. Secondly, the non dimensional constants,

$$\mathbb{P} = \frac{a_r T_\infty^4}{\rho_\infty c_v T_\infty}, \qquad\qquad \mathbb{C} = \frac{c}{a_\infty},$$

represent the ratio of material energy to radiation energy in the problem and the ratio of the speed of light to the speed of sound in the material, respectively.

Asymptotic Analysis

Typically, the RHD model (i.e. the coupled Euler and radiation transport equations) are solved in an operator split fashion. In this method, the transport model equations are solved while coupled with a material internal energy equation that only contains the radiation-matter coupling terms:

$$\frac{\partial \rho e}{\partial t} = -\mathbb{P}\mathbb{C} S_{\mathrm{E}}. \tag{I.8}$$

The other terms in the material energy equation are then updated during the hydrodynamics solve, along with a momentum exchange correction. As part of this operator splitting procedure, the radiation solve is undertaken with density and velocity terms that were evaluated at a particular time level. It is these radiation equations with the quasi-static material velocity and density that we will perform an asymptotic analysis on.

The P_1 equations, above, coupled with Eq. (I.8), are to be scaled under the conditions that the absorption cross-section is very large,

$$\sigma \to \frac{\sigma}{\epsilon}\,,$$

and where the ratio of the speed of light to the speed of sound is also very large,

$$\mathbb{C} \to \frac{\mathbb{C}}{\epsilon},$$

where ϵ is a "small", positive scaling parameter to be further defined below. These substitutions indicate that we are considering only asymptotic solutions to the transport equation for a system where the absorption mean free path is very small and the material reacts much quicker to changes in radiation than any material effects such as sound waves. Substituting these relationships into Equations (I.6) and (I.7) gives,

$$\epsilon\frac{\partial E_{\mathrm{r}}}{\partial t} + \mathbb{C}\nabla\cdot F_{\mathrm{r}} = \mathbb{C}S_{\mathrm{E}} \tag{I.9a}$$

$$\epsilon\frac{\partial F_{\mathrm{r}}}{\partial t} + \frac{1}{3}\mathbb{C}\nabla E_{\mathrm{r}} = \mathbb{C}S_{\mathrm{F}} \tag{I.9b}$$

$$\epsilon\frac{\partial \rho e}{\partial t} = -\mathbb{P}\mathbb{C}S_{\mathrm{E}} \tag{I.9c}$$

where the sources are now given by:

$$S_{\mathrm{E}} = \frac{\sigma}{\epsilon}\left(T^4 - E_{\mathrm{r}}\right) + \sigma\frac{v}{\mathbb{C}}\cdot F_{\mathrm{r0}}\,, \tag{I.10a}$$

$$S_{\mathrm{F}} = -\frac{\sigma}{\epsilon}F_{\mathrm{r0}} + \sigma\frac{v}{\mathbb{C}}\left(T^4 - E_{\mathrm{r}}\right)\,, \tag{I.10b}$$

$$F_{\mathrm{r0}} = F_{\mathrm{r}} - \frac{\epsilon}{\mathbb{C}}\left(vE_{\mathrm{r}} + \frac{v}{3}E_{\mathrm{r}}\right)\,. \tag{I.10c}$$

These scalings hold true for many nonrelativistic HEDP flows and all flows described in this work. All unknown variables in Eq. (I.9) and Eq. (I.10) are now expanded with a formal power series of the scaling constant ϵ. For example:

$$E_\mathrm{r} = \sum_{n=0}^{\infty} \epsilon^n E_\mathrm{r}^{(n)}, \qquad\qquad T^4 = \sum_{n=0}^{\infty} \epsilon^n T_{(n)}^4.$$

We will now look at the coefficients for each power of ϵ. The three orders of S_E are:

$$S_\mathrm{E}^{(-1)} = \sigma \left(T_{(0)}^4 - E_\mathrm{r}^{(0)} \right), \tag{I.11a}$$

$$S_\mathrm{E}^{(0)} = \sigma \left(T_{(1)}^4 - E_\mathrm{r}^{(1)} \right) + \sigma \frac{v}{\mathbb{C}} \cdot F_{\mathrm{r}0}^{(0)}, \tag{I.11b}$$

$$S_\mathrm{E}^{(1)} = \sigma \left(T_{(2)}^4 - E_\mathrm{r}^{(2)} \right) + \sigma \frac{v}{\mathbb{C}} \cdot F_{\mathrm{r}0}^{(1)}. \tag{I.11c}$$

Similarly for S_F:

$$S_\mathrm{F}^{(-1)} = -\sigma F_{\mathrm{r}0}^{(0)}, \tag{I.12a}$$

$$S_\mathrm{F}^{(0)} = -\sigma F_{\mathrm{r}0}^{(1)} + \sigma \frac{v}{\mathbb{C}} \left(T_{(0)}^4 - E_\mathrm{r}^{(0)} \right), \tag{I.12b}$$

$$S_\mathrm{F}^{(1)} = -\sigma F_{\mathrm{r}0}^{(2)} + \sigma \frac{v}{\mathbb{C}} \left(T_{(1)}^4 - E_\mathrm{r}^{(1)} \right). \tag{I.12c}$$

After inspecting Eqs. (I.9), it can be seen that no terms involve ϵ^{-1}. This shows that the $O(\epsilon^{-1})$ equations are equal to zero, therefore $S_\mathrm{E}^{(-1)} = S_\mathrm{F}^{(-1)} = 0$. Because of this, Eq. (I.11a) gives

$$T_{(0)}^4 = E_\mathrm{r}^{(0)}, \tag{I.13}$$

and Eq. (I.12a) gives

$$F_{\mathrm{r}0}^{(0)} = 0. \tag{I.14}$$

Gathering only the terms involving no power of ϵ in the P_1 equations, also known as $O(1)$ equations, is as follows:

$$\mathbb{C} \nabla \cdot F_\mathrm{r}^{(0)} = \mathbb{C} S_\mathrm{E}^{(0)} \tag{I.15a}$$

$$\frac{1}{3}\mathbb{C}\nabla E_{\mathrm{r}}^{(0)} = \mathbb{C}S_{\mathrm{F}}^{(0)} \tag{I.15b}$$

$$F_{\mathrm{r}0}^{(0)} = F_{\mathrm{r}}^{(0)} = 0 \tag{I.15c}$$

Equation (I.15a) reduces to $S_{\mathrm{E}}^{(0)} = 0$ due to Eq. (I.15c). Furthermore, this simplifies Eq. (I.11b) to

$$T_{(1)}^{4} = E_{\mathrm{r}}^{(1)}. \tag{I.16}$$

The first-order equation for $F_{\mathrm{r}0}$ is

$$F_{\mathrm{r}0}^{(1)} = F_{\mathrm{r}}^{(1)} - \frac{1}{\mathbb{C}}\left[vE_{\mathrm{r}}^{(0)} + \frac{v}{3}E_{\mathrm{r}}^{(0)}\right] \tag{I.17}$$

Substituting this relationship and Eq. (I.12b) into Eq. (I.15b) gives,

$$\frac{1}{3}\nabla E_{\mathrm{r}}^{(0)} = -\sigma F_{\mathrm{r}}^{(1)} + \frac{4}{3}\frac{v}{\mathbb{C}}\sigma E_{\mathrm{r}}^{(0)}, \tag{I.18}$$

after some algebra. Solving for $F_{\mathrm{r}}^{(1)}$ yields Fick's Law with an additional advection term:

$$F_{\mathrm{r}}^{(1)} = \frac{4}{3}\frac{v}{\mathbb{C}}E_{\mathrm{r}}^{(0)} - \frac{1}{3\sigma}\nabla E_{\mathrm{r}}^{(0)}. \tag{I.19}$$

Next, we look at the $O(\epsilon)$ equations arising from Eqs. (I.9):

$$\frac{\partial E_{\mathrm{r}}^{(0)}}{\partial t} + \mathbb{C}\nabla \cdot F_{\mathrm{r}}^{(1)} = \mathbb{C}S_{\mathrm{E}}^{(1)}, \tag{I.20a}$$

$$-\frac{1}{\mathbb{P}}\frac{\partial \rho e^{(0)}}{\partial t} = \mathbb{C}S_{\mathrm{E}}^{(1)}. \tag{I.20b}$$

Substituting Eq. (I.19) into Eq. (I.20a) gives

$$\frac{\partial E_{\mathrm{r}}^{(0)}}{\partial t} + \frac{1}{3}\nabla \cdot \left[4vE_{\mathrm{r}}^{(0)} - \frac{\mathbb{C}}{\sigma}\nabla E_{\mathrm{r}}^{(0)}\right] = \mathbb{C}S_{\mathrm{E}}^{(1)}. \tag{I.21}$$

Manipulating Eq. (I.21) with Eq. (I.15c) and rearranging gives

$$\frac{1}{\mathbb{P}}\frac{\partial \rho e^{(0)}}{\partial t} + \frac{\partial E_{\mathrm{r}}^{(0)}}{\partial t} + \frac{4}{3}\nabla v E_{\mathrm{r}}^{(0)} = \nabla \cdot \frac{\mathbb{C}}{3\sigma}\nabla E_{\mathrm{r}}^{(0)}. \tag{I.22}$$

Finally, this can be given in terms of material temperature due to Eq. (I.13):

$$\frac{1}{\mathbb{P}}\frac{\partial \rho e^{(0)}}{\partial t} + \frac{\partial T_{(0)}^4}{\partial t} + \frac{4}{3}\nabla v T_{(0)}^4 = \nabla \cdot \frac{\mathbb{C}}{3\sigma}\nabla T_{(0)}^4. \tag{I.23}$$

This is a conservation equations for material and radiative energy. The third term accounts for material motion through v, and is known as the drift term. This term would be absent without material motion. The term on the right hand side of the equation accounts for the diffusion of radiation energy. Therefore for a known density and material velocity (as outlined previously through an operator split scheme) the only dependent variable in this equation is the material temperature. This is the equilibrium drift-diffusion equation.

CHAPTER II

PROBLEM FORMULATION

The Marshak Wave

A long-standing example of non-linear radiative transfer is the Marshak wave, first described by Marshak in 1958 [6]. This wave is characterized by a self-similar profile that has typically been treated with a thermal diffusion approximation. This approximation is adequate in many situations. The material density and specific heat are constant while the opacity - or absorption cross-section - follows a power law dependent on material temperature. The problem geometry is a slab of material from $x \geq 0$ that is initially cold (close to zero temperature), and at $t = 0$ radiation is applied at the $x = 0$ surface and remains constant thereafter. This drives a thermal wave through the cold material. The wave propagating through the material is fundamentally different than other waves, such as an acoustic wave. It is a wave in the sense that a sharp temperature front moves through the material as a function of time. Its propagation law is distance $\propto$ time$^{1/2}$, which is typical of diffusive energy transport. In terms of similarity variables, the solution has a constant shape. It is this profile that we will compute.

Historically, when treating such problems, hydrodynamic motion has been ignored [6–9]. However, this work aims to include motion in the treatment of Marshak waves. Material motion adds significant complexity to the problem due to the fact that momentum conservation, and consequently energy transfer, depend on the relative velocity between the photons and the material. Adding material motion to Marshak wave problem is the next logical step in the advancement of verification codes.

Radiation Wave Front Approximation

In slab geometry, the equilibrium drift-diffusion equation, with subscripts removed is

$$\frac{d}{dt}\left(\rho e + \mathbb{P}T^4\right) + \frac{d}{dx}\left(\frac{4\mathbb{P}T^4}{3}u\right) = \frac{d}{dx}\frac{\mathbb{C}\mathbb{P}}{3\sigma}\frac{d}{dx}T^4. \tag{II.1}$$

A fundamental characteristic of the Marshak wave is its self-similar nature. Self-similarity is defined as a profile that is has a similar or exact shape as one or more parts of itself. In other words, the whole object has the same shape as one or more of its parts. If you zoom into a small section of the wave, and then transpose its shape over the entire wave profile, they will have the same shape. A similarity transform will be performed using,

$$\xi = \frac{Ax}{\sqrt{t}}, \qquad\qquad u = \frac{\theta U}{\sqrt{t}},$$

where A and θ are constants to be defined later, ξ is the scaled independent variable and u is the scaled material velocity. These transforms are suggested by understanding that distance $\propto$ time$^{1/2}$. We have prescribed a unique velocity profile, yet have not asserted how this would be formed. We simply state that if velocity follows a $1/\sqrt{t}$ dependence then self-similar solutions are possible. Although this may not seem physical or even beneficial, it is important to note that this velocity dependence can easily be prescribed in a simulation code. Simulation code verification is the premise of our study, therefore we feel this velocity prescription is valuable.

Implementing these transforms results in,

$$-\xi\frac{d}{d\xi}\left(\rho e + \mathbb{P}T^4\right) + \frac{8}{3}AU\theta\mathbb{P}\frac{d}{d\xi}T^4 = \frac{2A^2\mathbb{C}\mathbb{P}}{3}\frac{d}{d\xi}\frac{1}{\sigma}\frac{d}{d\xi}T^4. \tag{II.2}$$

Formally introducing the temperature-dependent cross section,

$$\sigma = \kappa_0 T^{-n}, \tag{II.3}$$

and substituting into Eq. (II.1) gives

$$-\xi\frac{d}{d\xi}\left(\rho e+\mathbb{P}T^4\right)+\frac{8}{3}AU\theta\mathbb{P}\frac{d}{d\xi}T^4=\frac{8A^2\mathbb{C}\mathbb{P}}{3(n+4)\kappa_0}\frac{d^2}{d\xi^2}T^{(n+4)}. \tag{II.4}$$

The exponent n for the cross-section can be set to $n=0$ to model electron scattering or to $n=3$ to model bound-free and free-free absorption reactions. It should also be noted that Eq. (II.3), with $n>0$, reveals that as the temperature increases the material becomes more transparent. From the nondimensionalization scheme, it can be seen that

$$\rho e=\frac{\rho c_v\hat{T}}{c_vT_\infty}=\rho T. \tag{II.5}$$

Therefore, by inserting this expression, Eq. (II.4) becomes,

$$-\xi\frac{d}{d\xi}\left(\rho T+\mathbb{P}T^4\right)+\frac{8}{3}AU\theta\mathbb{P}\frac{d}{d\xi}T^4=\frac{8A^2\mathbb{C}\mathbb{P}}{3(n+4)\kappa_0}\frac{d^2}{d\xi^2}T^{(n+4)}, \tag{II.6}$$

At this point the following constants will be defined to simplify the arithmetic:

$$U=\frac{3}{8A}, \tag{II.7a}$$

$$A^2=\frac{3(n+4)\kappa_0}{8\mathbb{C}\mathbb{P}}. \tag{II.7b}$$

Then, substituting Eq. (II.7b) into Eq. (II.7a) gives

$$U=\left[\frac{3\mathbb{C}\mathbb{P}}{8(n+4)\kappa_0}\right]^{1/2}. \tag{II.8}$$

Using these relationships, Eq. (II.4) simplifies to

$$-\xi\frac{d}{d\xi}\left(T+\mathbb{P}T^4\right)+\mathbb{P}\theta\frac{d}{d\xi}T^4=\frac{d^2}{d\xi^2}T^{(n+4)}. \tag{II.9}$$

In the limit $\mathbb{P}\to 0$, i.e. assuming radiation energy is negligible, this differential equation becomes equivalent to Eq. (12.7) on page 296 in [9] and Eq. (1) in [8]. A salient feature of

this equation is that although $\mathbb{P}$ is also a part of the right hand side of the expression, $\mathbb{C}$ limits this term from tending towards zero as $\mathbb{P} \to 0$. This equation is to be solved with the boundary condition that $T = T_0$ at $\xi = 0$, and another condition that maintains the temperature ahead of the wave front is sufficiently cold. Solutions of Eq. (II.9) go to zero at a finite value of ξ. This value of ξ will be referred to as ξ_{max}. For a particular value of ξ_{max}, there are an infinite number of solutions that tend to zero. However, only one of these solutions maintains a zero flux in the limit $\xi \to \xi_{max}$. Castor outlines an iterative numerical procedure beginning with an initial guess for ξ_{max} to determine the wave temperature profile. This value for ξ_{max} must be adjusted until an integration from ξ_{max} back to 0 gives $T(0) = T_0$. We now detail how to approximate the wave front location, ξ_{max}.

Integrating both sides, over $\xi < \xi' < \xi_{max}$, gives

$$-\xi \left(T(\xi') + \mathbb{P}T^4(\xi')\right)\Big|_{\xi}^{\xi_{max}} + \int_{\xi}^{\xi_{max}} \left(T(\xi') + \mathbb{P}T^4(\xi')\right)\, d\xi' + \mathbb{P}\theta T^4(\xi')\Big|_{\xi}^{\xi_{max}} = \frac{d}{d\xi}T^{(n+4)}(\xi')\Big|_{\xi}^{\xi_{max}}. \tag{II.10}$$

Simplifying using $T(\xi_{max}) = 0$ yields

$$\xi \left(T(\xi) + \mathbb{P}T^4(\xi)\right) + \int_{\xi}^{\xi_{max}} \left(T(\xi') + \mathbb{P}T^4(\xi')\right)\, d\xi' - \mathbb{P}\theta T^4(\xi) = -\frac{d}{d\xi}T^{(n+4)}(\xi). \tag{II.11}$$

For conciseness, the function $g(\xi) = T(\xi) + \mathbb{P}T^4(\xi)$ is defined and from this, the mean value of $g(\xi)$ from ξ to ξ_{max} can also be defined as

$$\bar{g}(\xi) = \frac{1}{\xi_{max} - \xi} \int_{\xi}^{\xi_{max}} g(\xi')\, d\xi'. \tag{II.12}$$

Using this relationship allows one to write the first two terms of Eq. (II.11) as

$$\xi g(\xi) + \int_{\xi}^{\xi_{max}} g(\xi')\, d\xi' = \xi_{max} g(\xi) - (\xi_{max} - \xi)\left(g(\xi) + \bar{g}(\xi)\right). \tag{II.13}$$

Then, due to the fact that $(\xi_{max} - \xi) \ll \xi_{max}$ near the shock front, the second term can be neglected. Therefore, Eq. (II.13) reduces to,

$$\xi g(\xi) + \int_{\xi}^{\xi_{max}} g(\xi')\, d\xi' \approx \xi_{max} g(\xi). \tag{II.14}$$

Nelson and Reynolds illustrate the previous approximation in Eqs. 6 & 7 of [8] and state that the relative error is of order $(\xi_{max} - \xi)/\xi_{max}$. Modulo this error, Eq. (II.11) reduces to

$$\xi_{max} \left[T(\xi) + \mathbb{P}T^4(\xi)\right] - \mathbb{P}\theta T^4(\xi) = -\frac{d}{d\xi} T^{(n+4)}(\xi). \tag{II.15}$$

Notice that through the chain rule,

$$(n+4) T^{(n+3)}(\xi) \frac{d}{d\xi} T(\xi) = \frac{d}{d\xi} T^{(n+4)}(\xi). \tag{II.16}$$

Because of this, Eq. (II.15) can be rewritten as

$$\xi_{max} \left[T(\xi) + \mathbb{P}T^4(\xi)\right] - \mathbb{P}\theta T^4(\xi) = -(n+4) T^{(n+3)}(\xi) \frac{d}{d\xi} T(\xi). \tag{II.17}$$

Dividing both sides by $T(\xi)$ gives

$$\xi_{max} \left[1 + \mathbb{P}T^3(\xi)\right] - \mathbb{P}\theta T^3(\xi) = -(n+4) T^{(n+2)}(\xi) \frac{d}{d\xi} T(\xi). \tag{II.18}$$

Now, applying a reverse application of the chain rule gives

$$\xi_{max} \left[1 + \mathbb{P}T^3(\xi)\right] - \mathbb{P}\theta T^3(\xi) = -\frac{(n+4)}{(n+3)} \frac{d}{d\xi} T^{(n+3)}(\xi). \tag{II.19}$$

This reduces to

$$\xi_{max} + \left[\xi_{max} - \theta\right] \mathbb{P}T^3(\xi) = -\frac{(n+4)}{(n+3)} \frac{d}{d\xi} T^{(n+3)}(\xi). \tag{II.20}$$

A final integration over ξ and again taking advantage of the fact that $T(\xi_{max}) = 0$ gives

$$\xi_{max}(\xi_{max} - \xi) + \mathbb{P}\left[\xi_{max} - \theta\right] \int_{\xi}^{\xi_{max}} T^3(\xi')\, d\xi' = \frac{(n+4)}{(n+3)} T^{(n+3)}(\xi). \tag{II.21}$$

Furthermore, evaluating the remaining integral using right-hand Riemann sums yields

$$\int_{\xi}^{\xi_{max}} T^3(\xi') d\xi' = (\xi_{max} - \xi) T^3(\xi_{max}) = 0, \tag{II.22}$$

due to $T^3(\xi_{max}) = 0$. This method maintains accuracy to order $(\xi_{max} - \xi)/\xi_{max}$. Eq. (II.21) now reduces to,

$$\xi_{max}\left(\xi_{max} - \xi\right) = \frac{(n+4)}{(n+3)} T^{(n+3)}(\xi). \tag{II.23}$$

Solving this equation for $T(\xi)$ provides an initial temperature approximation which is defined as $T_1(\xi)$:

$$T_1(\xi) = \left[\frac{(n+3)}{(n+4)} \xi_{max}\left(\xi_{max} - \xi\right)\right]^{1/(n+3)}. \tag{II.24}$$

With this temperature approximation we can evaluate the integral in Eq. (II.21) instead of using right-hand Riemann sums. This will generate a more accurate expression in which we will explicitly solve for $T(\xi)$ below. Substituting $T_1(\xi)$ into the integral term gives

$$\xi_{max}\left(\xi_{max} - \xi\right) + \mathbb{P}\left[\xi_{max} - \theta\right] \int_{\xi}^{\xi_{max}} \left[\frac{n+3}{n+4} \xi_{max}\left(\xi_{max} - \xi\right)\right]^{3/(n+3)} d\xi' = \frac{n+4}{n+3} T^{(n+3)}(\xi). \tag{II.25}$$

Evaluating the integral and simplifying yields

$$\xi_{max}\left(\xi_{max} - \xi\right) + \mathbb{P}\left[\xi_{max} - \theta\right] \frac{n+3}{n+6}\left(\xi_{max} - \xi\right) \left[\frac{n+3}{n+4} \xi_{max}\left(\xi_{max} - \xi\right)\right]^{\frac{3}{n+3}} = \frac{n+4}{n+3} T^{(n+3)}(\xi). \tag{II.26}$$

Solving explicitly for $T(\xi)$ gives a more accurate approximation, defined as $T_2(\xi)$:

$$T_2(\xi) = \left[\frac{n+3}{n+4}\left(\xi_{max} - \xi\right)\left(\xi_{max} + \mathbb{P}\frac{n+3}{n+6}\left(\xi_{max} - \theta\right)\left(\frac{n+3}{n+4} \xi_{max}\left(\xi_{max} - \xi\right)\right)^{3/(n+3)}\right)\right]^{1/(n+3)}. \tag{II.27}$$

This expression allows for a more accurate approximation of the radiation wave front moving through the cold medium. In the next section, ξ_{max} will be determined and tabulated for various values of $\mathbb{P}$ and θ under both $n = 0$ and $n = 3$. It is pertinent to expand on the definition of θ. By reflecting on its definition, one can see that it simply scales U to u. Therefore, θ can be seen as the ratio of the material velocity to the wave velocity. This constant is not merely an arbitrary quantity, it has physical relevance. To check validity of the previous expression, it is practical to compare to previous literature. Because no previous literature has included material motion in their solutions, we must make our solution comparable to the published results. Therefore, when $\mathbb{P} \to 0$, i.e. radiation energy is negligible, Eq. (II.27) becomes

$$T_2(\xi) = \left[\frac{n+3}{n+4}\xi_{max}\left(\xi_{max} - \xi\right)\right]^{1/(n+3)}, \tag{II.28}$$

which is identical to $T_1(\xi)$. In comparison, Nelson and Reynolds [8] claim,

$$g_2(\xi) = \left(\frac{(n+3)}{(n+4)}\left(\xi_{max} - \frac{1}{(n+4)}\frac{(\xi_{max} - \xi)}{2}\right)\left(\xi_{max} - \xi\right)\right)^{1/(n+3)}, \tag{II.29}$$

which agrees with Eq. (II.28) when one notes that $(\xi_{max} - \xi) \ll \xi_{max}$. This is important to illustrate because although our transport equations were different, due to the addition of material motion, when one makes the same assumptions as Nelson and Reynolds, these solutions will yield similar results. However, the added utility with our solution is that one is not forced to make those assumptions.

CHAPTER III

RESULTS

To solve for ξ_{max}, as well as the $T(\xi)$ profiles, the software *Wolfram Mathematica 9* was utilized. The solution procedure is as follows. We begin with an initial guess for ξ_{max} and then solve Eq. (II.9) using the boundary conditions $T(\xi_{max} - \delta) = T_2(\xi_{max} - \delta)$ and $T'(\xi_{max} - \delta) = T_2'(\xi_{max} - \delta)$. Then, based on whether $T(0)$ is greater than or less than 1, we adjust our guess for ξ_{max}. In our case $\delta = 10^{-10}$, while the functions `NDSolve` and `FindRoot` were used to integrate the ODE numerically and find the converged ξ_{max}. These calculations were performed at better-than-machine precision arithmetic by setting `WorkingPrecision` to 32. Before analyzing our new results, the author wanted to confirm the validity of previously known results. For this comparison, one must look at results that use the $T_1(\xi)$ approximation (shown in Eq. (II.24)). The $T_1(\xi)$ approximation inherently has no material motion therefore $\mathbb{P}$ and θ must be zero to provide comparable studies. In Castor's book, he claims $\xi_{max} = 1.232$ for $n = 0$ and $\xi_{max} = 1.121$ for $n = 3$ [9]. At the same precision, Nelson and Reynolds would claim 1.231 and 1.120, respectively [8]. Our results show $\xi_{max} = 1.231$ for $n = 0$ and $\xi_{max} = 1.119$ for $n = 3$. Therefore, the results calculated do align with previous literature and provide a reasonable sense of confidence in the other results of this study. The profiles for the benchmark problem are shown below in Fig. III.1.

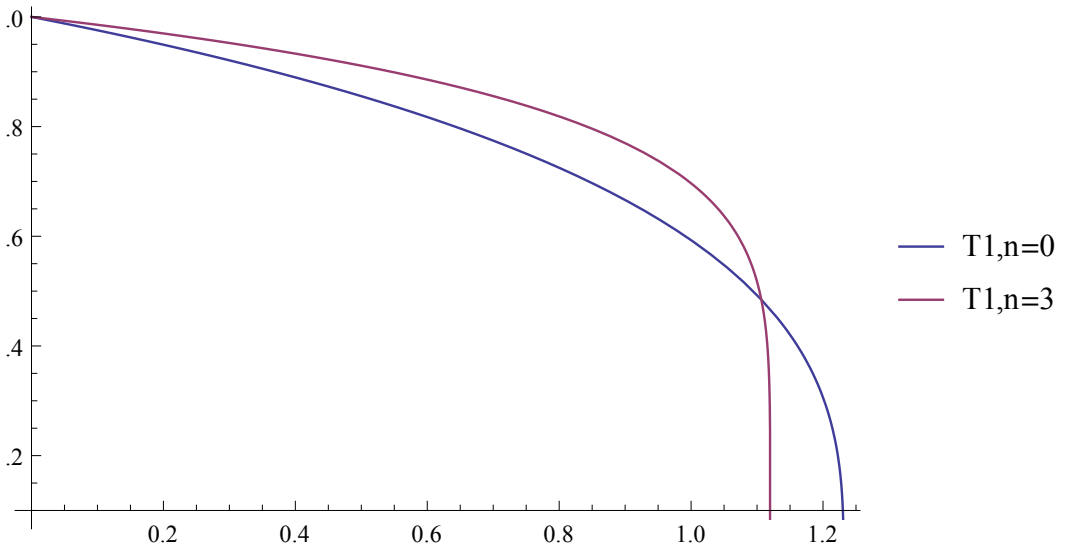

Fig. III.1. Benchmark Case Comparison for n = 0 and n = 3

From this figure it is easy to see that electron scattering problems have a flatter, less sharp wave front than do bound-bound and free-free problems. It can be said that the $n = 0$ case is more penetrating than $n = 3$. To look at the novel results now, various values for both $n = 0$ and $n = 3$ cases are presented in a tabulated format below in Table III.1. This figure shows nondimensional ξ on the abcissa and nondimensional temperature on the ordinate. These profiles are for a problem with no material motion. Progressiong to novel results, Table III.1 shows ξ_{max} values for a variety of material properties and speeds.

Table III.1
ξ_{max} for Motion Problems

θ	ξ_{max}					
	$\mathbb{P} = 0.04573$		$\mathbb{P} = 0.5$		$\mathbb{P} = 1$	
	$n = 0$	$n = 3$	$n = 0$	$n = 3$	$n = 0$	$n = 3$
10	1.36449	1.28213	3.57574	3.52816	5.19830	5.16451
5	1.28845	1.18959	2.07107	2.01057	2.83272	2.76374
2	1.24712	1.13852	1.40900	1.31516	1.57627	1.47967
1	1.23399	1.12220	1.25937	1.14168	1.28225	1.15790
0.1	1.22243	1.10780	1.14910	1.00925	1.08784	0.93103
0	1.22116	1.10621	1.13806	0.99582	1.06966	0.90931

This table sheds light on a few interesting features. It shows that as either θ or $\mathbb{P}$ increases, the wave grows. This is due to the fact that the advection term in Eq. (II.6) is scaled by $\mathbb{P}$. In the $\mathbb{P} = 0.04573$ case increasing θ from 10 to 0 has about a 15% effect in ξ_{max} for $n = 3$. The same change at $\mathbb{P} = 1$ leads to a 450% effect in ξ_{max}. Table III.1 also shows that as $\mathbb{P}$ becomes larger, or when the problem is in a radiation-dominated regime, the difference between wave front positions converges for both problems. Based on numerical results from $\mathbb{P}$ ranging from 0 to 2, we find that, for $\theta = 0$, ξ_{max} behaves as

$$\xi_{max} \approx 0.032\mathbb{P}^2 - 0.19\mathbb{P} + 1.2 \qquad n = 0, \tag{III.1}$$

$$\xi_{max} \approx 0.046\mathbb{P}^2 - 0.25\mathbb{P} + 1.1 \qquad n = 3. \tag{III.2}$$

Furthermore, Fig. III.2, below, show profiles of thermal waves with varying shock speeds which highlight these phenomena. The thermal wave profiles generated in Fig. III.2 are calculated for a sample problem where $a_r = 0.01372 \frac{\text{GJ}}{\text{keV}^4\text{-cm}^3}$, $T_\infty = 1$ keV, $\rho_\infty c_v = 0.3 \frac{\text{GJ}}{\text{keV-cm}^3}$, and $\kappa_0 = 300$ cm^{-1}. These values correspond to $\mathbb{P} = 0.04573$. This sample problem is a typical Marshak Wave solution and has appeared in the literature several times [10–12]. This value is used when calculating the profiles shown. To allows others to use these solutions for code verification we have included $T(\xi)$ for various values of θ at $\mathbb{P} = 0.04573$ in the appendix.

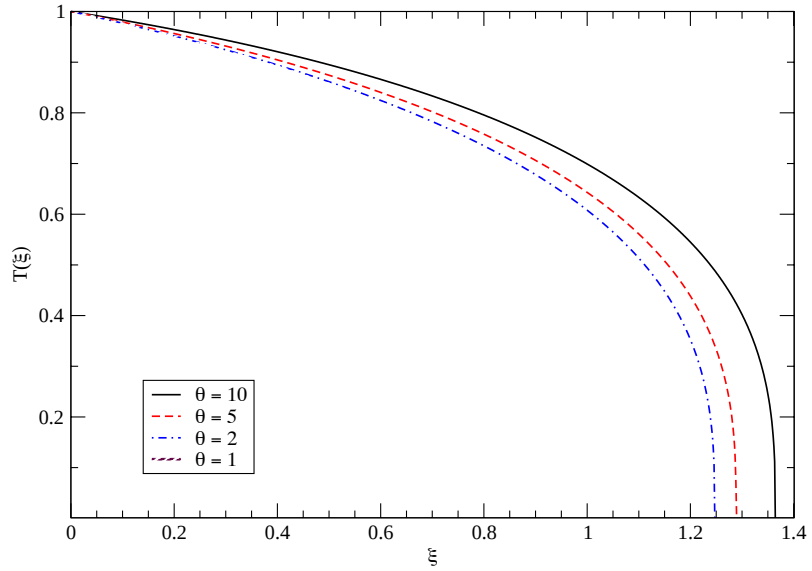

(a) $n = 0$

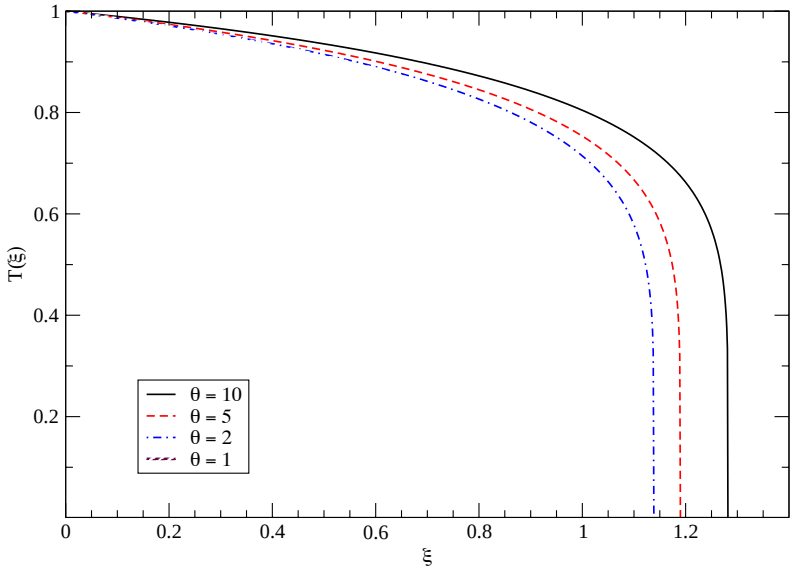

(b) $n = 3$

Fig. III.2. Self-similar thermal wave profiles for $\mathbb{P} = 0.04573$ with $n = 0$ and $n = 3$.

The differences between the two figures show that $n = 3$ profiles are more steep, which means the radiation is more penetrating, than the $n = 0$ problem. However, they both show that the difference between $\theta = 10$ and no material motion is certainly non-negligible.

To verify the validity of these results, we compared our results to an in-house numerical transport code [10, 13]. The results of the comparison can be found below in Fig. III.3. The numerical code results are shown as the red circles. It is illustrated that there's an appreciable difference between the two profiles which grows larger as time increases and the wave evolves. This figure is dimensionalized so that one can show the error grow as the wave and time increase. It shows profiles at 10, 20, and 50 nanoseconds. It is easy to see that the red circles follow the black line well. The black line shows our solutions including material motion while the blue line neglects it. Due to the two independent validations performed, the authors are reasonably confident in the novel solutions presented herein. However, the salient feature of this figure is the difference between including material motion in solutions and neglecting it. At 50 nanoseconds the wave has traveled approximately 0.38 cm. This is equivalent to a wave speed of 76 kilometers per second. The large wave speed is one reason that these wave profiles are difficult to study experimentally. This in turn puts more reliance on simulation codes and is the impetus of this study.

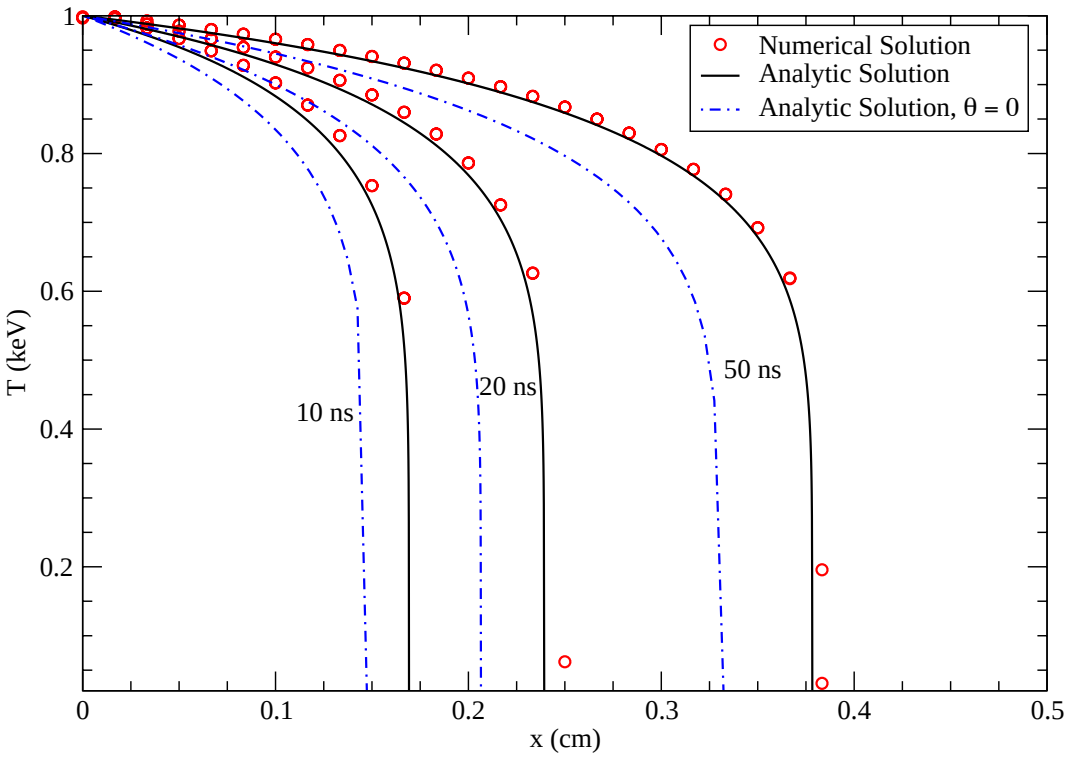

Fig. III.3. Comparison of a numerical solution to analytical self-similar solutions at various times to a Marshak wave problem with non-negligible radiation energy. The numerical and analytical solutions include material motion but the $\theta = 0$ curve does not.

CHAPTER IV
CONCLUSIONS

We have generalized the classic Marshak wave problem to include both radiation energy density terms and material motion. The material motion in our solutions is uniform in space and proportional to $t^{-1/2}$. In problems without any material motion, we observe that the greater the radiation energy density, as measured by the parameter $\mathbb{P}$, the slower the wave moves into the material. We phenomenologically quantified this effect with a quadratic in $\mathbb{P}$ model. We then showed that neglecting material motion accounts for an appreciable error in the position of the wave front that increases with time. To reduce this error we presented novel solutions to include material motion. Besides providing insight into the effects of radiation energy and material motion on Marshak waves, our solution can also be used to verify the radiation-material coupling treatment in a simulation code. Furthermore, this model could be implemented into codes to reduce the error due to this treatment. At the very least a study should be performed to determine for what values of θ are relevant to the problems currently being solved by these codes.

Future Work

The authors are currently studying the temporal evolution of these waves and how this evolution changes with material speed. Work is also currently being performed to analyze the effect of different materials on the wave profiles by varying the ρ_∞, T_∞, c_v, and κ_0 terms and relating them to physical experiments. This will test the model's fidelity by analyzing which parameters it is most sensitive to.

REFERENCES

[1] R. G. McClarren and J. G. Wöhlbier, "Solutions for ion-electron-radiation coupling with radiation and electron diffusion," *J. Quant. Spec. Rad. Transf.*, vol. 112, no. 1, pp. 119–130, 2010.

[2] R. B. Lowrie and J. E. Morel, "Issues with high-resolution Godunov methods for radiation hydrodynamics," *J. Quan. Spect. Rad. Trans.*, vol. 69, pp. 475–489, 2001.

[3] R. B. Lowrie, D. Mihalas, and J. Morel, "Comoving-frame radiation transport for non-relativistic fluid velocities," *J. Quant. Spec. Rad. Transf.*, vol. 69, pp. 291–304, 2001.

[4] D. Mihalas and B. Weibel-Mihalas, *Foundations of Radiation Hydrodynamics*. Mineola, New York: Dover Publications, 1999.

[5] G. L. Olson, L. H. Auer, and M. L. Hall, "Diffusion, P_1, and other approximate forms of radiation transport," *J. Quant. Spec. Rad. Transf.*, vol. 64, no. 6, pp. 619–634, 2000.

[6] R. E. Marshak, "Effect of radiation on shock wave behavior," *The Physics of Fluids*, vol. 1, no. 1, pp. 24–29, 1958.

[7] G. C. Pomraning, "The non-equilibrium Marshak wave problem," *J. Quant. Spec. Rad. Transf.*, pp. 249–261, 1979.

[8] E. M. Nelson and J. Reynolds, "Semi-analytic solution for a Marshak wave via numerical integration in Mathematica," tech. rep., Los Alamos National Laboratory, 2009.

[9] J. Castor, *Radiation Hydrodynamics*. Cambridge: Cambridge University Press, 2004.

[10] R. G. McClarren, T. M. Evans, R. B. Lowrie, and J. D. Densmore, "Semi-implicit time integration for P_N thermal radiative transfer," *J. Comput. Phys.*, vol. 227, no. 16, pp. 7561–7586, 2008.

[11] J. D. Edwards, J. E. Morel, and D. A. Knoll, "Nonlinear variants of the TR/BDF2 method for thermal radiative diffusion," *J. Comput. Phys.*, vol. 230, no. 4, pp. 1198–1214, 2011.

[12] E. W. Larsen, A. Kumar, and J. E. Morel, "Properties of the implicitly time-differenced equations of thermal radiation transport," *Progress in Nuclear Energy*, vol. 238, pp. 82–96, Apr. 2013.

[13] R. G. McClarren and R. B. Lowrie, "The effects of slope limiting on asymptotic-preserving numerical methods for hyperbolic conservation laws," *J. Comput. Phys.*, vol. 227, pp. 9711–9726, Jan 2008.

APPENDIX A

VERIFICATION TABLES

These tables are provided for others to use in the verification of simulation codes with the velocity dependence described within this work for $\mathbb{P} = 0.04573$, which corresponds to a typical sample problem, and values of $n = 0$ and $n = 3$.

Table A.1
Solutions $T(\xi)$ for a problem with $\mathbb{P} = 0.04573$ and $n = 0$.

	ξ	$\theta = 10$	$\theta = 5$	$\theta = 2$	$\theta = 1$	$\theta = 0.1$	$\theta = 0$
1	0.00000	1.00000	1.00000	1.00000	1.00000	1.00000	1.00000
2	0.02843	0.99534	0.99427	0.99359	0.99336	0.99316	0.99313
3	0.05685	0.99054	0.98840	0.98705	0.98659	0.98617	0.98612
4	0.08528	0.98562	0.98239	0.98035	0.97966	0.97903	0.97896
5	0.11371	0.98056	0.97623	0.97351	0.97258	0.97174	0.97165
6	0.14213	0.97535	0.96991	0.96650	0.96534	0.96429	0.96417
7	0.17056	0.97000	0.96344	0.95933	0.95793	0.95667	0.95652
8	0.19899	0.96450	0.95680	0.95199	0.95035	0.94887	0.94870
9	0.22742	0.95883	0.94999	0.94446	0.94259	0.94089	0.94070
10	0.25584	0.95300	0.94300	0.93675	0.93464	0.93272	0.93251
11	0.28427	0.94700	0.93582	0.92885	0.92649	0.92435	0.92412
12	0.31270	0.94082	0.92844	0.92074	0.91813	0.91578	0.91551
13	0.34112	0.93445	0.92086	0.91241	0.90956	0.90698	0.90669
14	0.36955	0.92788	0.91306	0.90387	0.90076	0.89795	0.89764
15	0.39798	0.92111	0.90503	0.89508	0.89172	0.88868	0.88834
16	0.42640	0.91412	0.89677	0.88604	0.88242	0.87915	0.87878
17	0.45483	0.90691	0.88826	0.87674	0.87286	0.86935	0.86896
18	0.48326	0.89946	0.87949	0.86716	0.86301	0.85926	0.85884
19	0.51168	0.89176	0.87043	0.85729	0.85287	0.84887	0.84842
20	0.54011	0.88379	0.86109	0.84710	0.84240	0.83815	0.83767
21	0.56854	0.87556	0.85143	0.83658	0.83159	0.82708	0.82658
22	0.59697	0.86702	0.84143	0.82571	0.82042	0.81564	0.81511
23	0.62539	0.85818	0.83109	0.81445	0.80885	0.80380	0.80324
24	0.65382	0.84901	0.82036	0.80278	0.79687	0.79153	0.79094
25	0.68225	0.83948	0.80923	0.79067	0.78443	0.77880	0.77817
26	0.71067	0.82958	0.79766	0.77808	0.77150	0.76556	0.76490
27	0.73910	0.81928	0.78561	0.76497	0.75803	0.75176	0.75107
28	0.76753	0.80855	0.77306	0.75129	0.74397	0.73736	0.73663
29	0.79595	0.79735	0.75994	0.73699	0.72927	0.72229	0.72151
30	0.82438	0.78565	0.74622	0.72200	0.71384	0.70647	0.70565
31	0.85281	0.77341	0.73182	0.70624	0.69762	0.68983	0.68896
32	0.88123	0.76057	0.71668	0.68962	0.68050	0.67223	0.67131
33	0.90966	0.74708	0.70071	0.67204	0.66235	0.65357	0.65259
34	0.93809	0.73287	0.68380	0.65335	0.64303	0.63367	0.63262
35	0.96652	0.71786	0.66583	0.63338	0.62234	0.61231	0.61119
36	0.99494	0.70196	0.64664	0.61190	0.60004	0.58923	0.58802
37	1.02337	0.68506	0.62603	0.58864	0.57580	0.56405	0.56274
38	1.05180	0.66701	0.60374	0.56320	0.54916	0.53625	0.53480
39	1.08022	0.64764	0.57943	0.53502	0.51946	0.50506	0.50343
40	1.10865	0.62672	0.55262	0.50329	0.48570	0.46925	0.46738
41	1.13708	0.60398	0.52262	0.46669	0.44621	0.42672	0.42448
42	1.16550	0.57901	0.48837	0.42290	0.39782	0.37313	0.37023
43	1.19393	0.55127	0.44808	0.36705	0.33301	0.29652	0.29196
44	1.22236	0.51995	0.39832	0.28479	0.22073	0.04126	-
45	1.25078	0.48378	0.33076	-	-	-	-
46	1.27921	0.44055	0.20740	-	-	-	-
47	1.30764	0.38573	-	-	-	-	-
48	1.33607	0.30686	-	-	-	-	-
49	1.36449	-	-	-	-	-	-

Table A.2
Solutions $T(\xi)$ for a problem with $\mathbb{P} = 0.04573$ and $n = 3$.

	ξ	$\theta = 10$	$\theta = 5$	$\theta = 2$	$\theta = 1$	$\theta = 0.1$	$\theta = 0$
1	0.00000	1.00000	1.00000	1.00000	1.00000	1.00000	1.00000
2	0.02671	0.99729	0.99677	0.99643	0.99632	0.99622	0.99620
3	0.05342	0.99452	0.99346	0.99279	0.99255	0.99234	0.99232
4	0.08013	0.99168	0.99007	0.98905	0.98870	0.98838	0.98834
5	0.10684	0.98877	0.98660	0.98522	0.98475	0.98432	0.98427
6	0.13356	0.98579	0.98305	0.98130	0.98070	0.98016	0.98010
7	0.16027	0.98273	0.97940	0.97728	0.97655	0.97589	0.97582
8	0.18698	0.97960	0.97567	0.97316	0.97229	0.97151	0.97142
9	0.21369	0.97638	0.97183	0.96892	0.96792	0.96701	0.96691
10	0.24040	0.97308	0.96789	0.96457	0.96343	0.96239	0.96228
11	0.26711	0.96968	0.96384	0.96010	0.95881	0.95764	0.95751
12	0.29382	0.96619	0.95967	0.95549	0.95406	0.95275	0.95260
13	0.32053	0.96261	0.95538	0.95075	0.94916	0.94771	0.94755
14	0.34724	0.95891	0.95097	0.94587	0.94412	0.94252	0.94234
15	0.37396	0.95511	0.94642	0.94083	0.93891	0.93716	0.93696
16	0.40067	0.95119	0.94172	0.93563	0.93354	0.93162	0.93141
17	0.42738	0.94715	0.93687	0.93026	0.92798	0.92589	0.92566
18	0.45409	0.94298	0.93186	0.92470	0.92222	0.91996	0.91971
19	0.48080	0.93867	0.92668	0.91893	0.91626	0.91381	0.91354
20	0.50751	0.93421	0.92131	0.91296	0.91007	0.90743	0.90713
21	0.53422	0.92960	0.91574	0.90675	0.90364	0.90079	0.90047
22	0.56093	0.92483	0.90996	0.90029	0.89694	0.89387	0.89353
23	0.58764	0.91987	0.90394	0.89356	0.88996	0.88665	0.88628
24	0.61435	0.91473	0.89767	0.88653	0.88266	0.87910	0.87870
25	0.64107	0.90938	0.89114	0.87918	0.87501	0.87119	0.87076
26	0.66778	0.90381	0.88430	0.87147	0.86699	0.86287	0.86240
27	0.69449	0.89800	0.87714	0.86336	0.85854	0.85410	0.85360
28	0.72120	0.89193	0.86962	0.85481	0.84962	0.84482	0.84429
29	0.74791	0.88558	0.86170	0.84577	0.84016	0.83498	0.83440
30	0.77462	0.87893	0.85335	0.83617	0.83011	0.82449	0.82386
31	0.80133	0.87193	0.84449	0.82594	0.81936	0.81325	0.81257
32	0.82804	0.86456	0.83508	0.81498	0.80782	0.80115	0.80039
33	0.85475	0.85678	0.82503	0.80318	0.79534	0.78801	0.78718
34	0.88147	0.84852	0.81424	0.79037	0.78174	0.77364	0.77272
35	0.90818	0.83975	0.80260	0.77637	0.76679	0.75775	0.75672
36	0.93489	0.83038	0.78995	0.76089	0.75015	0.73994	0.73877
37	0.96160	0.82032	0.77608	0.74358	0.73137	0.71965	0.71830
38	0.98831	0.80948	0.76072	0.72388	0.70973	0.69595	0.69435
39	1.01502	0.79770	0.74348	0.70094	0.68408	0.66729	0.66531
40	1.04173	0.78481	0.72379	0.67335	0.65235	0.63063	0.62801
41	1.06844	0.77058	0.70078	0.63837	0.61010	0.57849	0.57445
42	1.09515	0.75467	0.67293	0.58960	0.54424	0.47872	0.46807
43	1.12187	0.73661	0.63734	0.50300	0.26230	-	-
44	1.14858	0.71569	0.58696	-	-	-	-
45	1.17529	0.69073	0.49328	-	-	-	-
46	1.20200	0.65964	-	-	-	-	-
47	1.22871	0.61787	-	-	-	-	-
48	1.25542	0.55197	-	-	-	-	-
49	1.28213	0.01824	-	-	-	-	-